INTERNATIONAL JOURNAL FOR NUMERICAL METHODS IN FLUIDS
Int. J. Numer. Meth. Fluids 2008; **56**:331–350
Published online 4 July 2007 in Wiley InterScience (www.interscience.wiley.com). DOI: 10.1002/fld.1534

Numerical simulations of 3D free surface flows by a multilayer Saint-Venant model

E. Audusse[1], M. O. Bristeau[1,*,†] and A. Decoene[2]

[1]*INRIA, Domaine de Voluceau, BP 105, Le Chesnay 78153, France*
[2]*INRIA and LNHE, EDF, 6 Quai Watier, BP 49, Chatou 78401, France*

SUMMARY

We present a multilayer Saint-Venant system for the simulation of 3D free surface flows with friction and viscosity effects. A vertical discretization of a Navier–Stokes system approximation deduced from a precise analysis of the shallow water assumption leads to a set of coupled Saint-Venant-type systems. The idea is to obtain an accurate description of the vertical profile of the horizontal velocity while preserving the robustness and the computational efficiency of the usual Saint-Venant system.

For each time-dependent layer, a Saint-Venant-type system is solved on the same 2D mesh by a kinetic solver using a finite volume framework. The free surface is directly deduced from the sum of layers water depth.

We validate the model with some numerical academic and realistic examples. We present comparisons with simulations computed with the hydrostatic Navier–Stokes solver of the Telemac-3D code developed by Electricité de France. Copyright © 2007 John Wiley & Sons, Ltd.

Received 29 May 2006; Revised 10 April 2007; Accepted 20 April 2007

KEY WORDS: multilayer Saint-Venant system; free surface flows; hydrostatic assumption; finite volumes

1. INTRODUCTION

In this paper, we present a multilayer Saint-Venant system for the simulation of 3D free surface flows with friction and viscosity effects. The idea is to introduce, when the hydrostatic assumption is valid, an alternative to the solution of the free surface Navier–Stokes system, leading to a precise description of the vertical profile of the horizontal velocity while preserving the robustness and the computational efficiency of the usual Saint-Venant system.

This study generalizes the work of Audusse [1] who has developed a model based on the 1D Saint-Venant system for problems with flat bottom.

*Correspondence to: M. O. Bristeau, INRIA, Domaine de Voluceau, BP 105, Le Chesnay 78153, France.
†E-mail: Marie-Odile.Bristeau@inria.fr

Contract/grant sponsor: EDF/LNHE

The multilayer Saint-Venant system is deduced from the Navier–Stokes system by two steps:

- the shallow water assumption leading to the hydrostatic Navier–Stokes model;
- the vertical discretization of the flow domain and the vertical integration of this model on each layer.

For the first step, we refer to the study by Ferrari and Saleri [2] who have generalized the work of Gerbeau and Perthame [3] to 3D problems with slow varying bottom. For the second step, we only give the 2D result which is analogous to the one based on the 1D Saint-Venant system proved in [1].

Once the model is established, we emphasize in this paper the numerical approximation of the multilayer Saint-Venant system for the simulation of 3D flows, discussing with details the numerical implementation. The coupled Saint-Venant systems are solved by a kinetic solver on a finite volume discretization.

The free surface Navier–Stokes computations, which have to deal with a 3D moving mesh, are rather expensive. Here, we only use a 2D mesh, the time-dependent layers being managed by the Saint-Venant-type equations. The same idea has been applied in [4] with non-conservative Saint-Venant systems discretized by finite elements. Also the bi-fluid shallow water problem considered in [5] is treated as a two-layer flow.

We show on some example a comparison of the two approaches, multilayer system and hydrostatic Navier–Stokes equations. For the Navier–Stokes simulations we use the Telemac-3D code developed by Electricité de France (EDF) (see [6, 7]).

The outline of the paper is as follows. In Section 2, we recall the incompressible Navier–Stokes equations, the boundary conditions and the hydrostatic approximation. The multilayer Saint-Venant system obtained by a vertical discretization of the hydrostatic model is described in Section 3. The numerical scheme is presented in Section 4 and the boundary conditions in Section 5. In Section 6, we give some details on the postprocessing step. Numerical examples are shown in Section 7. The first one is academic so that we can compare precisely the solutions of the proposed multilayer system and of a hydrostatic Navier–Stokes code. The second one is realistic and aims to prove the robustness of the scheme.

2. NAVIER–STOKES EQUATIONS AND HYDROSTATIC APPROXIMATION

2.1. Navier–Stokes equations

We consider the classical incompressible Navier–Stokes system

$$\nabla \cdot \mathbf{U} = 0 \tag{1}$$

$$\frac{\partial \mathbf{U}}{\partial t} + \nabla \cdot (\mathbf{U} \otimes \mathbf{U}) = \nabla \cdot \sigma + \mathbf{g} \tag{2}$$

with the stress tensor σ given by

$$\sigma = -p\mathbb{I}d + \mu[\nabla \mathbf{U} + (\nabla \mathbf{U})^{\mathrm{T}}] \tag{3}$$

and where $\mathbf{U}(t, x, y, z) = (u, v, w)^{\mathrm{T}}$ is the velocity, $\mathbf{u}(t, x, y, z) = (u, v)^{\mathrm{T}}$ is the horizontal velocity, p is the pressure, $\mathbf{g} = (0, 0, -g)^{\mathrm{T}}$ represents the gravity forces and μ is the viscosity coefficient.

DOI: 10.1002/fld

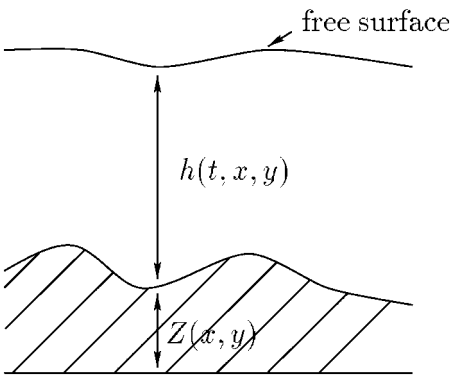

Figure 1. Flow domain.

We consider a free surface flow (see Figure 1), therefore we assume

$$Z(x, y) \leqslant z \leqslant H(t, x, y) = h(t, x, y) + Z(x, y)$$

with $Z(x, y)$ the bottom elevation and $h(t, x, y)$ the water depth.

On the bottom we prescribe an impermeability condition

$$\mathbf{U} \cdot \mathbf{n} = 0 \tag{4}$$

and a friction condition given by a Navier law

$$(\sigma \cdot \mathbf{n}) \cdot \mathbf{t}_i = -\kappa \mathbf{U} \cdot \mathbf{t}_i, \quad i = 1, 2 \tag{5}$$

with κ a Navier coefficient, $\mathbf{n}$ the unit outward normal and $(\mathbf{t}_i, i = 1, 2)$ two tangential vectors. For some applications, we rather use the Strickler friction and Equation (5) is then replaced by

$$(\sigma \cdot \mathbf{n}) \cdot \mathbf{t}_i = -K(h, \mathbf{U})\ \mathbf{U} \cdot \mathbf{t}_i, \quad i = 1, 2 \tag{6}$$

where $K(h, \mathbf{U}) = (g/S^2 h^{1/3}) \|\mathbf{U}\|$ with S the Strickler coefficient.

On the free surface, the kinematic boundary condition is satisfied

$$\frac{\partial H}{\partial t} + \mathbf{u}(t, x, y, H) \cdot \nabla H - w(t, x, y, H) = 0 \tag{7}$$

and the no-stress condition

$$\boldsymbol{\sigma} \cdot \mathbf{n} = 0 \tag{8}$$

On solid walls, we prescribe a slip condition

$$\mathbf{U} \cdot \mathbf{n} = 0 \tag{9}$$

We complete this system with some initial conditions

$$h(0, x, y) = h^0(x, y), \quad \mathbf{U}(0, x, y, z) = \mathbf{U}^0(x, y, z)$$

DOI: 10.1002/fld

2.2. Hydrostatic model

We introduce the shallow water assumption. For this purpose we consider two characteristic dimensions $\mathscr{H}$ and $\mathscr{L}$ in the vertical and horizontal directions respectively and we assume that $\mathscr{H}$ is small compared to $\mathscr{L}$, so we can write $\varepsilon = \mathscr{H}/\mathscr{L}$ with ε a small parameter. We also assume a slow-varying bottom [2]. We introduce dimensionless variables and we obtain a dimensionless Navier–Stokes system (see [1, 2, 8]). By an asymptotic analysis, we deduce the approximation at zero order in ε of system (1)–(9) which gives the horizontally inviscid hydrostatic model

$$\nabla \cdot \mathbf{U} = 0 \tag{10}$$

$$\frac{\partial \mathbf{u}}{\partial t} + \nabla \cdot (\mathbf{u} \otimes \mathbf{u}) + \frac{\partial \mathbf{u} w}{\partial z} + \nabla p = \mu \frac{\partial^2 \mathbf{u}}{\partial z^2} \tag{11}$$

$$\frac{\partial p}{\partial z} = -g \tag{12}$$

with the boundary conditions

$$w(t, x, y, Z(x, y)) = 0 \tag{13}$$

$$\mu \frac{\partial \mathbf{u}}{\partial z}(t, x, y, Z(x, y)) = \kappa \mathbf{u}(t, x, y, Z(x, y)) \tag{14}$$

$$\frac{\partial \mathbf{u}}{\partial z}(t, x, y, H(t, x, y)) = 0 \tag{15}$$

$$p(t, x, y, H(t, x, y)) = 0 \tag{16}$$

The system is still associated with the kinematic boundary condition (7).

Taking into account the pressure boundary condition on the free surface (16), Equation (12) is equivalent to

$$p(t, x, y, z) = g(H(t, x, y) - z) \tag{17}$$

3. A MULTILAYER SAINT-VENANT SYSTEM

3.1. Multilayer system

In order to define a vertical discretization of system (10)–(16), we introduce a discretization of the water domain in the z direction (see Figure 2). For some $M \in \mathbb{N}$ we define M intermediate water heights $H_\alpha(t, x, y)$ such that

$$0 = H_0(t, x, y) \leqslant H_1(t, x, y) \leqslant H_2(t, x, y) \leqslant \cdots \leqslant H_{M-1}(t, x, y) \leqslant H_M(t, x, y) = h(t, x, y)$$

Then for each layer we define its water height $h_\alpha(t, x, y)$ by

$$\forall \alpha \in \{1, M\}, \quad h_\alpha(t, x, y) = H_\alpha(t, x, y) - H_{\alpha-1}(t, x, y)$$

DOI: 10.1002/fld

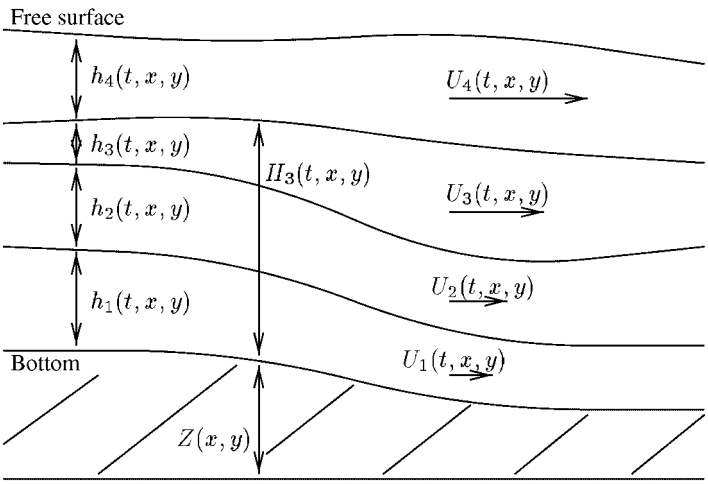

Figure 2. Water domain discretization in the z direction.

and so

$$\sum_{\alpha=1}^{M} h_\alpha(t,x,y) = h(t,x,y)$$

We assume that the interfaces are advected by the flow.

We also define an average horizontal velocity $\mathbf{U}_\alpha(t,x,y)$ by

$$\forall \alpha \in \{1,M\}, \quad \mathbf{U}_\alpha(t,x,y) = \frac{1}{h_\alpha(t,x,y)} \int_{H_{\alpha-1}}^{H_\alpha} \mathbf{u}(t,x,y,z)\,\mathrm{d}z \tag{18}$$

The 1D theorem analogous to the following has been proved in [1].

Theorem 3.1

The multilayer Saint-Venant system with friction defined by

$$\frac{\partial h_\alpha}{\partial t} + \nabla \cdot (h_\alpha \mathbf{U}_\alpha) = 0 \tag{19}$$

$$\begin{aligned} &\frac{\partial h_\alpha \mathbf{U}_\alpha}{\partial t} + \nabla \cdot (h_\alpha \mathbf{U}_\alpha \otimes \mathbf{U}_\alpha) + g h_\alpha \nabla h \\ &\quad = -g h_\alpha \nabla Z - \kappa_\alpha \mathbf{U}_\alpha + 2\mu_\alpha \frac{\mathbf{U}_{\alpha+1} - \mathbf{U}_\alpha}{h_{\alpha+1} + h_\alpha} \\ &\qquad - 2\mu_{\alpha-1} \frac{\mathbf{U}_\alpha - \mathbf{U}_{\alpha-1}}{h_\alpha + h_{\alpha-1}} \quad \text{for } \alpha = 1, \ldots, M \end{aligned} \tag{20}$$

with

$$\kappa_\alpha = \begin{cases} \kappa & \text{if } \alpha = 1 \\ 0 & \text{if } \alpha \neq 1 \end{cases}, \quad \mu_\alpha = \begin{cases} 0 & \text{if } \alpha = 0 \\ \mu & \text{if } \alpha = 1, \ldots, M-1 \\ 0 & \text{if } \alpha = M \end{cases}$$

DOI: 10.1002/fld

results from a formal asymptotic approximation in $O(\varepsilon)$, coupled with a vertical discretization, of the hydrostatic model and therefore of the Navier–Stokes equations.

Remark
It is noticeable that, thanks to the kinematic boundary condition at each interface, the vertical velocity is no more a variable of system (20). This is an advantage of this formulation over the hydrostatic model where the vertical velocity is needed in the momentum equation (11) and is deduced from the incompressibility condition (10). Here it is deduced from the same condition (see Section 6.2) but it is decoupled, it is already the case for the Saint-Venant system [3].

The multilayer Saint-Venant system satisfies some fundamental properties (see [1]). We only mention here that the multilayer system (19)–(20) preserves the positivity of the water height in each layer. It also preserves the steady state of still water, i.e. $h+Z=Cst$, $\mathbf{u}=0$. When $Z=Cst$, the total momentum is conserved.

3.2. Conservative form

However, the formulation of the multilayer system (19)–(20) has two main drawbacks. The pressure terms $h_\alpha \nabla h$ are not in a conservative form and thus their definition is not obvious in the presence of shocks. Several definitions of these non-conservative products have been proposed [9] depending on which discontinuities to reproduce. Here the outcome is to preserve the above properties and stability.

In addition, if we consider a two-layer system satisfying

$$\mathbf{U}_\alpha(t,x,y)=\mathbf{U}(t,x,y)+O(\varepsilon) \quad \forall \alpha=1,2 \tag{21}$$

we verify (see [1]) that this two-layer system is not hyperbolic.

This has motivated in [1] the following new set-up of the same system with a conservative form of the left-hand side:

$$\frac{\partial h_\alpha}{\partial t}+\nabla\cdot(h_\alpha \mathbf{U}_\alpha)=0 \tag{22}$$

$$\begin{aligned}\frac{\partial h_\alpha \mathbf{U}_\alpha}{\partial t}&+\nabla(h_\alpha \mathbf{U}_\alpha\otimes\mathbf{U}_\alpha)+\frac{g}{2}\nabla(h_\alpha h)\\ &=\frac{g}{2}h^2\nabla\left(\frac{h_\alpha}{h}\right)-gh_\alpha\nabla Z-\kappa_\alpha\mathbf{U}_\alpha+2\mu_\alpha\frac{\mathbf{U}_{\alpha+1}-\mathbf{U}_\alpha}{h_{\alpha+1}+h_\alpha}\\ &\quad-2\mu_{\alpha-1}\frac{\mathbf{U}_\alpha-\mathbf{U}_{\alpha-1}}{h_\alpha+h_{\alpha-1}} \quad \text{for } \alpha=1,\ldots,M\end{aligned} \tag{23}$$

If we denote $\mathbf{X}_\alpha=(h_\alpha,\mathbf{q}_\alpha)^{\mathrm{T}}$ with $\mathbf{q}_\alpha=h_\alpha\mathbf{U}_\alpha$ or $\mathbf{q}_\alpha=(q_{\alpha,x},q_{\alpha,y})^{\mathrm{T}}$, system (22)–(23) can be written:

$$\frac{\partial \mathbf{X}_\alpha}{\partial t}+\nabla\cdot\mathbf{F}(h,\mathbf{X}_\alpha)=\mathbf{B}_p(h,\mathbf{X}_\alpha)+\mathbf{B}_z(\mathbf{X}_\alpha)+\mathbf{B}_v(\mathbf{X}_{\alpha-1},\mathbf{X}_\alpha,\mathbf{X}_{\alpha+1}) \quad \text{for } \alpha=1,\ldots,M \tag{24}$$

DOI: 10.1002/fld

with

$$\mathbf{F}(h,\mathbf{X}_\alpha)=\begin{pmatrix} q_{\alpha,x} & q_{\alpha,y} \\ \dfrac{q_{\alpha,x}^2}{h_\alpha}+\dfrac{g}{2}h_\alpha h & \dfrac{q_{\alpha,x}q_{\alpha,y}}{h_\alpha} \\ \dfrac{q_{\alpha,x}q_{\alpha,y}}{h_\alpha} & \dfrac{q_{\alpha,y}^2}{h_\alpha}+\dfrac{g}{2}h_\alpha h \end{pmatrix} \tag{25}$$

$$\mathbf{B}_p(h,\mathbf{X}_\alpha)=\begin{pmatrix} 0 \\ \dfrac{g}{2}h^2\partial_x\left(\dfrac{h_\alpha}{h}\right) \\ \dfrac{g}{2}h^2\partial_y\left(\dfrac{h_\alpha}{h}\right) \end{pmatrix}, \quad \mathbf{B}_z(\mathbf{X}_\alpha)=\begin{pmatrix} 0 \\ -gh_\alpha\partial_x Z \\ -gh_\alpha\partial_y Z \end{pmatrix} \tag{26}$$

and

$$\mathbf{B}_v(\mathbf{X}_{\alpha-1},\mathbf{X}_\alpha,\mathbf{X}_{\alpha+1})=\begin{pmatrix} 0 \\ -\kappa_\alpha\mathbf{U}_\alpha+2\mu_\alpha\dfrac{\mathbf{U}_{\alpha+1}-\mathbf{U}_\alpha}{h_{\alpha+1}+h_\alpha}-2\mu_{\alpha-1}\dfrac{\mathbf{U}_\alpha-\mathbf{U}_{\alpha-1}}{h_\alpha+h_{\alpha-1}} \end{pmatrix} \tag{27}$$

4. NUMERICAL SCHEME

In this section, we detail the space and time discretization of system (24)–(27).

4.1. Time discretization

With Δt the time step, knowing the solution $(\mathbf{X}_\alpha^n, \alpha=1,\ldots,M)$ at time $t^n=n\Delta t$, we compute the solution at time t^{n+1} with an explicit treatment of the hyperbolic part (left-hand side), the non-conservative pressure source term $\mathbf{B}_p$ and the bottom topography term $\mathbf{B}_z$, and with an implicit treatment of the viscous and friction terms $\mathbf{B}_v$, so that the scheme is written

$$\frac{\mathbf{X}_\alpha^{n+1}-\mathbf{X}_\alpha^n}{\Delta t}+\nabla\cdot\mathbf{F}(h^n,\mathbf{X}_\alpha^n)=\mathbf{B}_p(h^n,\mathbf{X}_\alpha^n)+\mathbf{B}_z(\mathbf{X}_\alpha^n)+\mathbf{B}_v(\mathbf{X}_{\alpha-1}^{n+1},\mathbf{X}_\alpha^{n+1},\mathbf{X}_{\alpha+1}^{n+1}) \tag{28}$$

We note that h_α^{n+1} is obtained explicitly since the first component of $\mathbf{B}_v$ is 0 and that $\mathbf{U}_\alpha^{n+1}$ is the solution of a tridiagonal $M\times M$ linear system (see [1] for details of the matrix terms).

4.2. Space discretization

Concerning the space discretization, we consider finite volumes defined on an unstructured mesh. We recall here the general formalism of finite volumes. Let $\mathscr{T}_h$ be a triangulation of the computational domain which vertices are denoted P_i. The dual cells C_i are obtained by joining the

DOI: 10.1002/fld

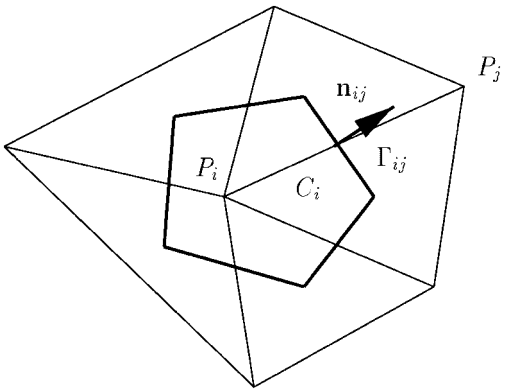

Figure 3. Dual cell C_i.

centres of mass of the triangles surrounding each vertex P_i. We use the following notations (see Figure 3):

- K_i, set of subscripts of nodes P_j surrounding P_i;
- $|C_i|$, area of the cell C_i;
- $\mathscr{T}_i$, set of triangles T_k having P_i as a node;
- $|T_k|$, area of the triangle T_k;
- Γ_{ij}, boundary edge between the cells C_i and C_j;
- L_{ij}, length of Γ_{ij};
- $\mathbf{n}_{ij}$, unit normal to Γ_{ij}, outward to C_i ($\mathbf{n}_{ji} = -\mathbf{n}_{ij}$).

We denote by $\mathbf{X}^n_{\alpha,i} = (h^n_{\alpha,i}, \mathbf{q}^n_{\alpha,i})$ an approximation of the cell average of the solution at time t^n. The space discretization of system (28) gives after integration on the cell C_i

$$\mathbf{X}^{n+1}_{\alpha,i} + \Delta t \mathbf{B}_v(\mathbf{X}^{n+1}_{\alpha-1,i}, \mathbf{X}^{n+1}_{\alpha,i}, \mathbf{X}^{n+1}_{\alpha+1,i}) = \mathbf{X}^n_{\alpha,i} - \sum_{j\in K_i} \sigma_{ij}\, \mathscr{F}(h^n_{ij}, h^n_{ji}, \mathbf{X}^n_{\alpha,ij}, \mathbf{X}^n_{\alpha,ji}, \mathbf{n}_{ij}) + \Delta t \mathbf{S}_{p,i}(h^n, \mathbf{X}^n_\alpha, (h^n_{ij},\, j \in K_i)) + \sum_{j\in K_i} \sigma_{ij} \mathbf{S}_z(h^n_i, h^n_{ij}, \mathbf{X}^n_{\alpha,i}, \mathbf{X}^n_{\alpha,ij}, \mathbf{n}_{ij}) \tag{29}$$

with $\sigma_{ij} = \Delta t L_{ij}/|C_i|$.

We develop in the following subsections the definition of the different terms of the right-hand side of Equation (29).

4.3. Flux term

For the hyperbolic part, the term $\mathscr{F}(h_{ij}, h_{ji}, \mathbf{X}_{\alpha,ij}, \mathbf{X}_{\alpha,ji}, \mathbf{n}_{ij})$ denotes an interpolation of the normal component of the flux $\mathbf{F}(h, \mathbf{X}_\alpha)\cdot\mathbf{n}_{ij}$ (appearing after integration by parts of the divergence term) along the edge Γ_{ij}. The fluxes at the interfaces are computed by a kinetic solver analogous to the one described in detail in [10] for the Saint-Venant system. Here the Gibbs equilibrium for

DOI: 10.1002/fld

the layer α is

$$M_\alpha(t,x,y,\xi)=\frac{h_\alpha(t,x,y)}{c^2(t,x,y)}\chi\left(\frac{\xi-\mathbf{U}_\alpha(t,x,y)}{c(t,x,y)}\right) \tag{30}$$

with

$$c(t,x,y)=\sqrt{\frac{gh(t,x,y)}{2}}$$

and the notations defined in [10]. This has the advantage of simple explicit formulas that are very stable (both theoretically and numerically). But other choices of the solver could be used as well here [11].

The interface values $h_{ij}, h_{ji}, \mathbf{X}_{\alpha,ij}, \mathbf{X}_{\alpha,ji}$ are defined in the next subsection in such a way that the bottom topography term preserves the steady state of still water.

4.4. Topography term

The interface values $h_{ij}, h_{ji}, \mathbf{X}_{\alpha,ij}, \mathbf{X}_{\alpha,ji}$ are computed using the hydrostatic reconstruction proposed in [12]. The different steps are as follows.

We define:

- a piecewise constant approximation of the bottom topography $Z(x,y)$

$$Z_i=\frac{1}{|C_i|}\int_{C_i} Z(x,y)\,\mathrm{d}x\mathrm{d}y \tag{31}$$

- an interface topography (we denote by Z_{ij}, Z_{ji} the values at the interface between nodes P_i and P_j)

$$Z_{ij}=Z_{ji}=\max(Z_i,Z_j) \tag{32}$$

- a hydrostatic reconstructed total water depth

$$h_{ij}=(h_i+Z_i-Z_{ij})_+ \tag{33}$$

- a proportional reconstructed water depth for each layer

$$h_{\alpha,ij}=h_{\alpha,i}\frac{h_{ij}}{h_i}\quad\text{and}\quad \mathbf{q}_{\alpha,ij}=h_{\alpha,ij}\mathbf{U}_\alpha \tag{34}$$

Then, we define the term $\mathbf{S}_z(h_i,h_{ij},\mathbf{X}_{\alpha,i},\mathbf{X}_{\alpha,ij},\mathbf{n}_{ij})$ (which is an approximation by interface of the bottom source term $\mathbf{B}_z$) by the formula

$$\mathbf{S}_z(h_i,h_{ij},\mathbf{X}_{\alpha,i},\mathbf{X}_{\alpha,ij},\mathbf{n}_{ij})=\begin{pmatrix}0\\ \dfrac{g}{2}(h_{\alpha,ij}+h_{\alpha,i})(h_{ij}-h_i)\mathbf{n}_{ij}\end{pmatrix} \tag{35}$$

Following [10], we can prove that scheme (29) preserves the still water steady state.

DOI: 10.1002/fld

4.5. Non-conservative pressure term

To complete the definition of the scheme given by (29), it remains to define the term $\mathbf{S}_{p,i}(h, \mathbf{X}_\alpha, (h_{ij}, j \in K_i))$ which is an approximation of the non-conservative source term of the right-hand side $\mathbf{B}_p$ defined in (26).

As we have node values for h_α/h, we can consider a piecewise linear approximation on the triangles and we denote $\nabla(h_\alpha/h)|_{T_k}$ the constant gradient on each triangle surrounding the node P_i. Then, we define a centred approximation of the gradient term by a weighted average

$$\nabla\left(\frac{h_\alpha}{h}\right)\Big|_i = \frac{1}{\sum |T_k|} \sum_{T_k \in \mathscr{T}_i} |T_k| \ \nabla\left(\frac{h_\alpha}{h}\right)\Big|_{T_k} \tag{36}$$

For consistency with the other terms, we use for the approximation of h^2 the reconstructed water depth h_{ij} but, as it is defined by interface, we use as node value the minimum of the surrounding values, so we obtain the following formula:

$$\mathbf{S}_{p,i}(h, \mathbf{X}_\alpha, (h_{ij}, j \in K_i)) = \begin{pmatrix} 0 \\ \dfrac{g}{2} \min\limits_{j \in K_i}(h_{ij}^2) \nabla\left(\dfrac{h_\alpha}{h}\right)\Big|_i \end{pmatrix} \tag{37}$$

5. BOUNDARY CONDITIONS

Concerning the boundary conditions we refer mainly to [13] where the treatment of the boundary conditions for the shallow water equations is detailed. The idea is to deduce from the boundary conditions the values to be prescribed for the variables on a fictitious outside cell, and thus to be able to apply the scheme at the boundary nodes (in order to preserve the properties of the scheme at these nodes). We explain here how these conditions can be generalized to deduce boundary conditions for each layer of the multilayer system, since only global conditions are generally given at the fluid boundaries.

5.1. Inflow boundary

As an example we assume that a global inflow flux Q_g is given.

For each boundary node, we assume a one-layer model and we deduce the values $h_{e,i}, \mathbf{U}_{e,i}$ on the fictitious outside cell using the algorithm proposed in [13] and based on the conservation of the outgoing Riemann invariant. Then, we prescribe

$$h_{e,\alpha,i} = \frac{h_{e,i}}{M} \quad \text{for } \alpha = 1, \ldots, M \tag{38}$$

For the velocity components, we assume either a constant velocity along the vertical direction, i.e. $\mathbf{U}_{e,\alpha,i} = \mathbf{U}_{e,i}$, or a parabolic vertical profile. In the last case, the parabolic profile $\mathbf{u}_i(z)$ is defined by the three conditions (we use (14), (15)):

$$\frac{\partial \mathbf{u}_i}{\partial z}(z) = 0 \quad \text{for } z = h_{e,i} \tag{39}$$

DOI: 10.1002/fld

$$\frac{\partial \mathbf{u}_i}{\partial z}(z) = k\mathbf{u}_i(z) \quad \text{for } z=0 \text{ with } k=\kappa/\mu \tag{40}$$

$$\int_0^{h_e} \mathbf{u}_i(z)\,\mathrm{d}z = h_{e,i}\mathbf{U}_{e,i} \tag{41}$$

and we define

$$\mathbf{U}_{e,\alpha,i} = \int_{(\alpha-1)h_{e,\alpha,i}}^{\alpha h_{e,\alpha,i}} \mathbf{u}_i(z)\,\mathrm{d}z \tag{42}$$

5.2. *Outflow boundary*

For the outflow boundary, a usual condition is to prescribe the water depth h_{g}.

As in the previous case, we assume a one-layer model and we compute the values $h_{e,i}, \mathbf{U}_{e,i}$ to be prescribed on the fictitious outside cell. Then, for each layer, we prescribe

$$h_{e,\alpha,i} = h_{\alpha,i}\frac{h_{e,i}}{h_i}, \quad \mathbf{U}_{e,\alpha,i} = \mathbf{U}_{\alpha,i}\frac{\mathbf{U}_{e,i}}{\mathbf{U}_i} \tag{43}$$

where $\mathbf{U}_i$ is the average value of velocity for the total water depth

$$\mathbf{U}_i = \frac{1}{h_i}\sum_{\alpha=1}^{M} h_{\alpha,i}\mathbf{U}_{\alpha,i} \tag{44}$$

5.3. *Slip condition*

On a solid wall the slip condition

$$\mathbf{U}_{\alpha,i}\cdot\mathbf{n}_i = 0 \tag{45}$$

is prescribed weakly (see [13]) for each layer.

6. POSTPROCESSING COMPUTATIONS

6.1. *3D outputs*

The computation of the solution of the multilayer system deals only with the 2D mesh, but for the output plottings, it is easier to define the velocity components at the nodes of a 3D mesh and then to use linear interpolation for the isovalues. From the 2D mesh, the bottom data and the water depth of each layer we deduce a 3D mesh made of prisms which can then be divided into a tetrahedra. Along the vertical direction the nodes of the 3D mesh are located at the bottom, at the middle of each layer and at the free surface (see Figure 4). We assign to the nodes $P_{i,\alpha}$ in the layer α the value of the horizontal velocity $\mathbf{U}_{\alpha,i} = (U_{\alpha,i}, V_{\alpha,i})^{\mathrm{T}}$. The values of the horizontal velocity at the bottom (denoted $(U_{0,i}, V_{0,i})^{\mathrm{T}}$) and at the free surface $(U_{M+1,i}, V_{M+1,i})^{\mathrm{T}}$ are computed by linear extrapolation along the vertical direction.

DOI: 10.1002/fld

6.2. Vertical velocity

The vertical velocity is not a variable of the multilayer system, nevertheless, it may be interesting to compute it for the outputs and the comparisons with Navier–Stokes solutions. It is deduced from the impermeability condition (4) at the bottom and the integration along the z-axis of the incompressibility condition (1).

We define $\mathbf{n}_i = (n_{x,i}, n_{y,i}, n_{z,i})^{\mathrm{T}}$, the unit normal at each node of the bottom, by an average (weighted by the areas of the faces) of the surrounding face normals, then the vertical velocity is defined at each node of the bottom by

$$W_{0,i} = -\frac{1}{n_{z,i}}(U_{0,i} n_{x,i} + V_{0,i} n_{y,i}) \tag{46}$$

The incompressibility condition implies for the continuous variables

$$w(x, y, z) = w(x, y, Z) - \int_Z^z \left(\frac{\partial u}{\partial x} + \frac{\partial v}{\partial y}\right) \mathrm{d}z \tag{47}$$

thus, for the discrete variables, we write

$$W_{\alpha,i} = W_{0,i} - \sum_{k=1}^{\alpha-1} h_{k,i} \left(\left.\frac{\partial U_k}{\partial x}\right|_i + \left.\frac{\partial V_k}{\partial y}\right|_i\right) - \frac{h_{\alpha,i}}{2}\left(\left.\frac{\partial U_\alpha}{\partial x}\right|_i + \left.\frac{\partial V_\alpha}{\partial y}\right|_i\right) \tag{48}$$

where

$$\left.\frac{\partial U_k}{\partial x}\right|_i = \frac{1}{\sum |T_j|} \sum_{T_j \in \mathscr{T}_i} |T_j| \left.\frac{\partial U_k}{\partial x}\right|_{T_j} \tag{49}$$

with $(\partial U_k/\partial x)|_{T_j}$ the constant x-derivative by triangle of U_k considered as piecewise linear.

6.3. Wet-dry interface

It is not necessary to define the position of the wet–dry interface for the computations since the scheme can deal with cells where the water depth is zero. However, for CPU time savings, it may be interesting to avoid the flux computation for the cell interfaces with zero water depth on each side.

Nevertheless, since the computational variable is the discharge $\mathbf{q}_{\alpha,i}$ and the velocity is needed for the computation of (29), we have to introduce a threshold value ε_h in order to define the velocity everywhere. Therefore, we set

$$\mathbf{U}_{\alpha,i} = \begin{cases} \dfrac{\mathbf{q}_{\alpha,i}}{h_{\alpha,i}} & \text{if } h_{\alpha,i} \geqslant \varepsilon_h \\ 0 & \text{else} \end{cases} \tag{50}$$

7. NUMERICAL RESULTS

We consider two types of test cases, an academic one and a realistic one, and for the two cases we present comparisons with Navier–Stokes solutions. We compare the results obtained with

DOI: 10.1002/fld

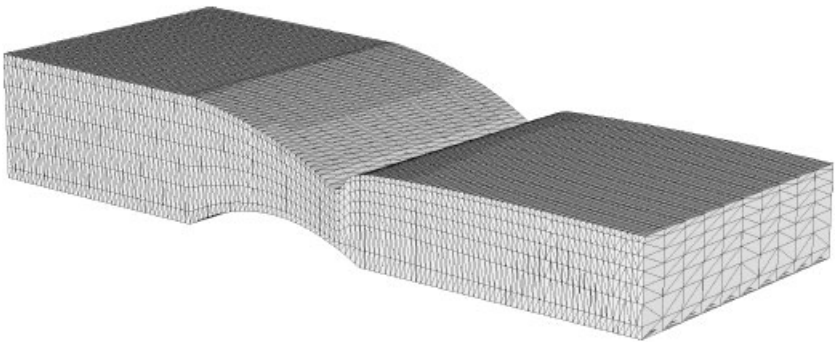

Figure 4. Flow over a bump. The 3D mesh for the postprocessing.

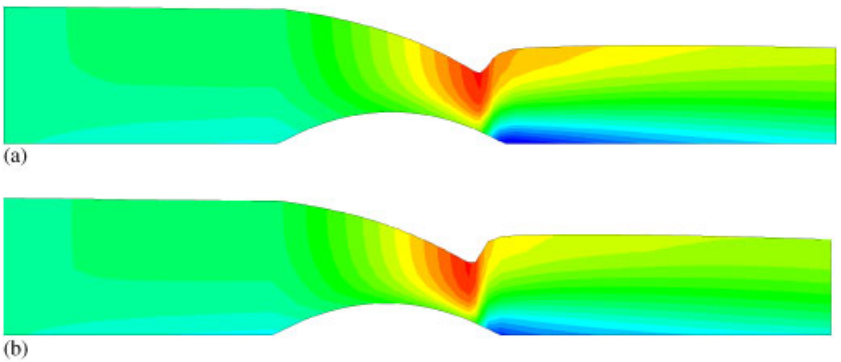

Figure 5. Horizontal velocities ($S = 30$): (a) multilayer Saint-Venant model and (b) hydrostatic Navier–Stokes model.

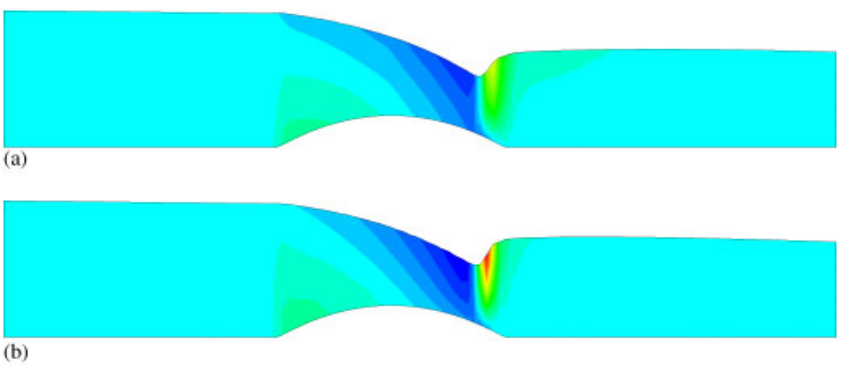

Figure 6. Vertical velocities ($S = 30$): (a) multilayer Saint-Venant model and (b) hydrostatic Navier–Stokes model.

DOI: 10.1002/fld

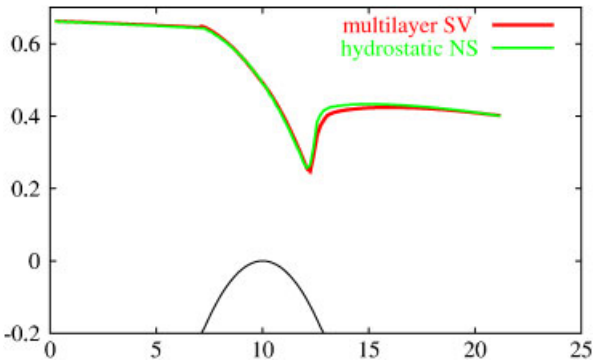

Figure 7. Free surface comparisons: multilayer Saint-Venant model (solid line) and hydrostatic Navier–Stokes model (tinted line).

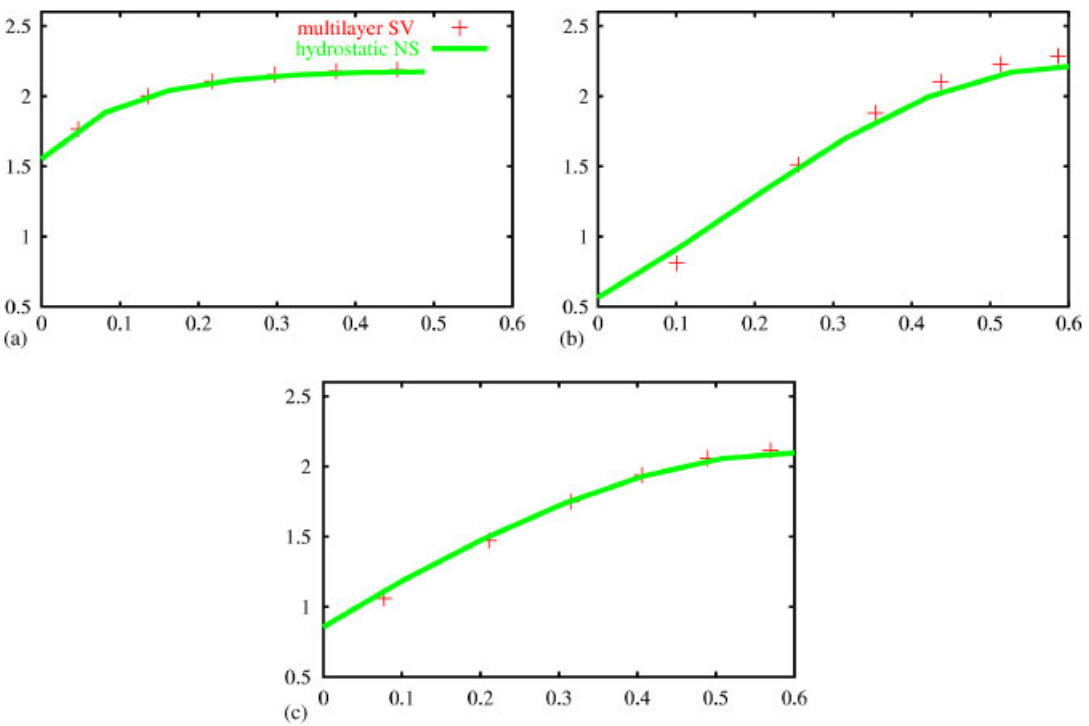

Figure 8. Vertical profiles of horizontal velocity: Comparison of the multilayer (crosses) and of the hydrostatic Navier–Stokes (continuous lines) solutions: (a) $x = 10$; (b) $x = 15$; and (c) $x = 20$.

the multilayer system described above and the hydrostatic Navier–Stokes solver 'Telemac-3D' described in [6, 7]. The main ingredients of the Telemac-3D solver are finite elements, operator splitting, semi-implicit scheme and σ transformation (A.L.E. type transformation) along the vertical axis.

DOI: 10.1002/fld

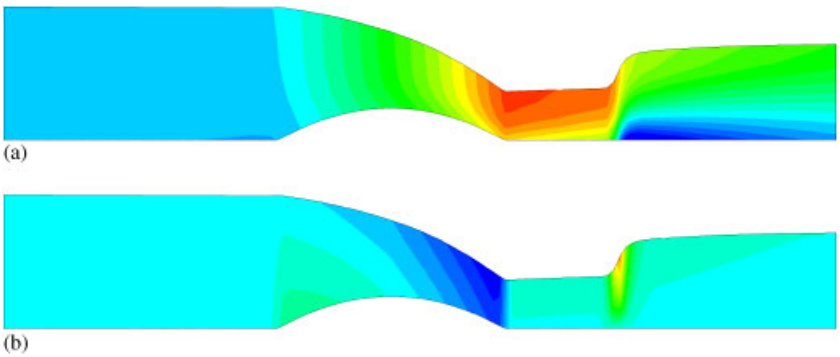

Figure 9. Multilayer Saint-Venant model ($S = 50$): (a) horizontal velocity and (b) vertical velocity.

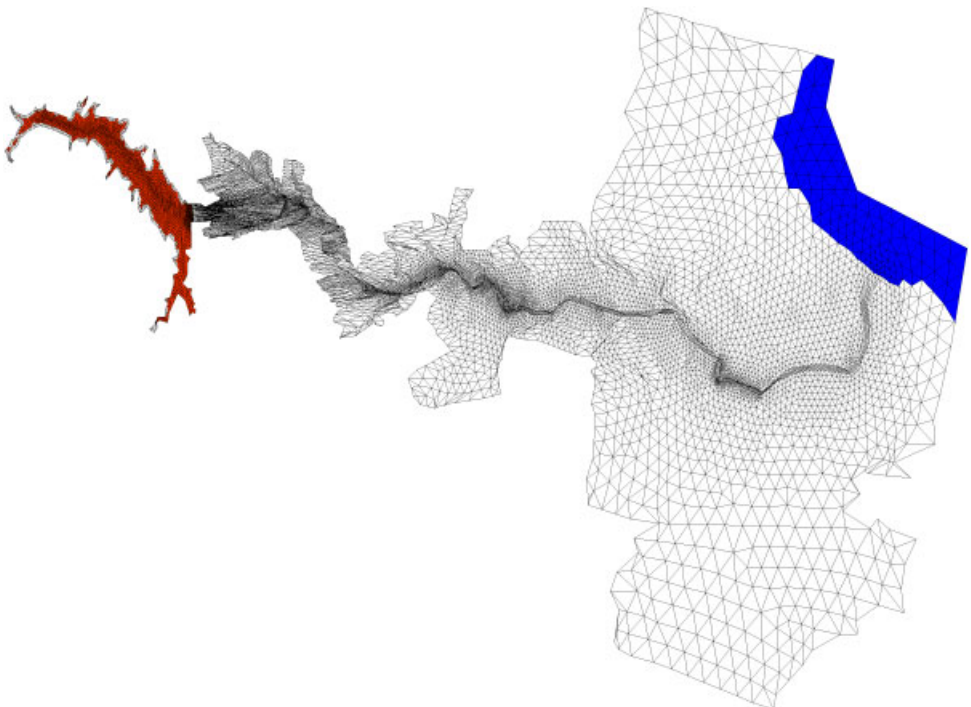

Figure 10. Malpasset: topography and initial solution.

7.1. Transcritical flow over a bump

We consider the classical test of a stationary transcritical flow over a parabolic bump. The geometric data are the following: channel length ≈ 21 m, channel width ≈ 2 m, bump length ≈ 5.75 m, bump height ≈ 0.2 m. At the inflow boundary, the given discharge is $2\,\mathrm{m}^3/\mathrm{s}$ and at the outflow the

DOI: 10.1002/fld

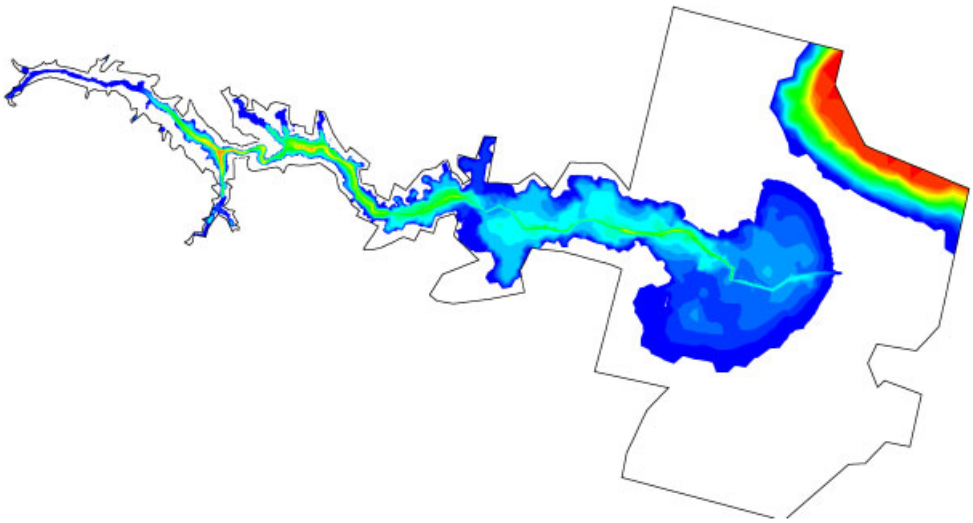

Figure 11. Malpasset: multilayer Saint-Venant model. Water depth at $t = 2500\,\mathrm{s}$.

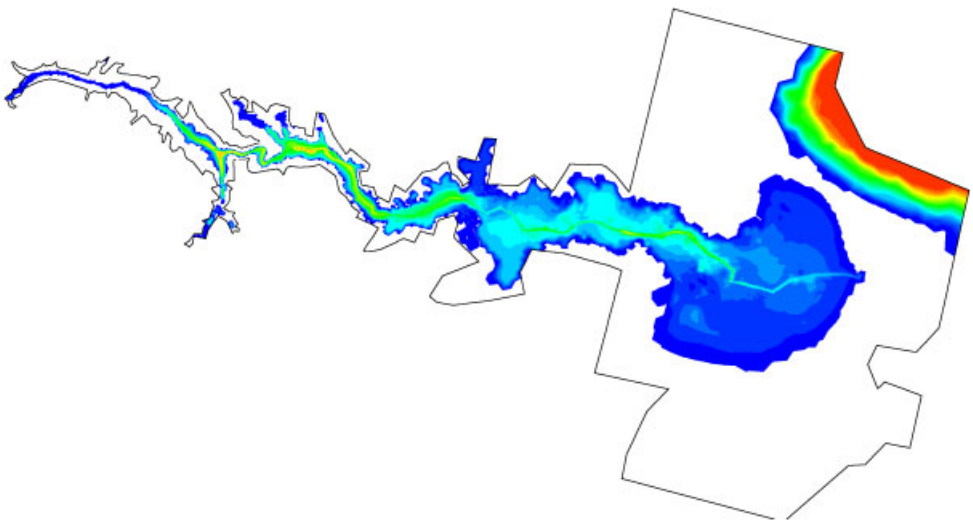

Figure 12. Malpasset: hydrostatic Navier–Stokes model. Water depth at $t = 2500\,\mathrm{s}$.

prescribed water depth is 0.6 m. The vertical viscosity is $10^{-2}\,\mathrm{m}^2/\mathrm{s}$ and the Strickler coefficient is 30.

The results shown in Figures 5–8 have been obtained with six layers along the vertical axis (1452 nodes, 2620 triangles for the 2D mesh). Figure 4 shows the 3D mesh built for the multilayer outputs as described in Section 6.1 (as we have half a layer at the bottom and at the free surface, this 3D mesh has seven layers). For the hydrostatic Navier–Stokes results, we use the six layers 3D mesh used for the computation.

DOI: 10.1002/fld

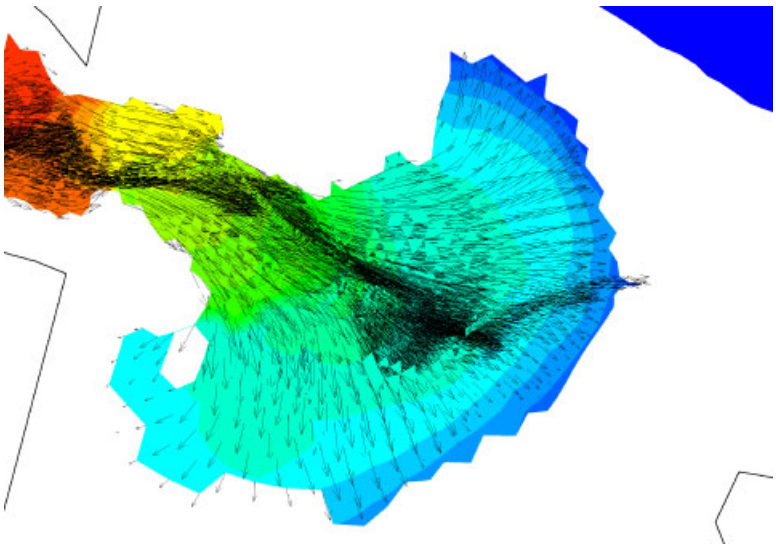

Figure 13. Malpasset: zoom of the downstream area. Multilayer Saint-Venant model. Water level and mean velocity at $t = 2500$ s.

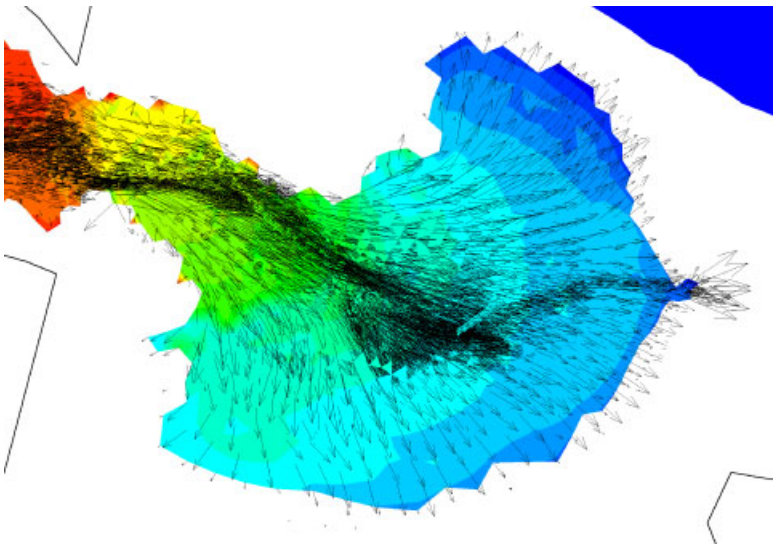

Figure 14. Malpasset: zoom of the downstream area. Hydrostatic Navier–Stokes model. Water level and mean velocity at $t = 2500$ s.

We compare in Figures 5–6 the horizontal and vertical components of the velocity. In Figure 8, we compare the vertical profiles of the horizontal velocity at different positions. We can see the good agreement of the results obtained with the two different models though the approximation

DOI: 10.1002/fld

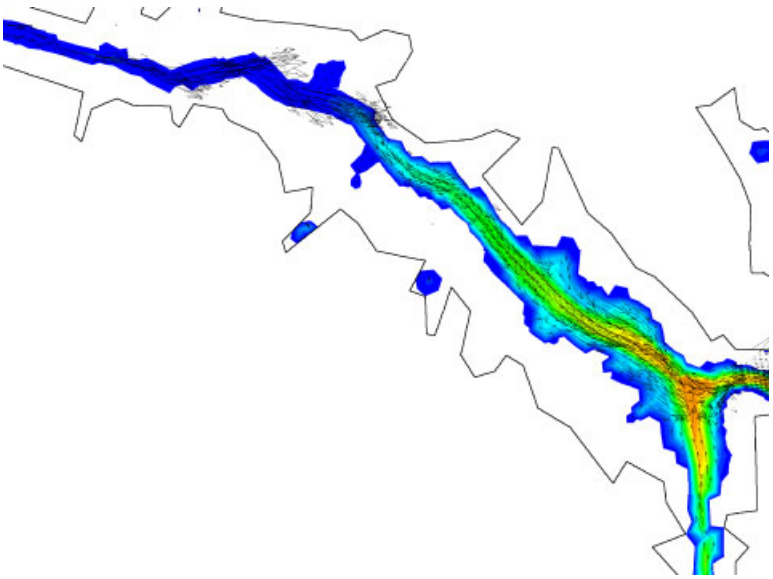

Figure 15. Malpasset: zoom of the upstream area. Water depth and mean velocity at $t = 2500$ s.

of the velocities are different (constant by layer or piecewise linear). The CPU times are 10 min for the multilayer and 33 min for the hydrostatic Navier–Stokes solver.

To show the effect of the friction coefficient, we have done a computation with the same data except the Strickler coefficient is now 50. The horizontal and vertical velocities are presented in Figure 9. As the friction is less important, the jump is further after the bump.

7.2. Malpasset

The second test problem is a real-life application, it concerns the Malpasset dam break. The circumstances of the event, the data of the numerical simulation and a solution by a Saint-Venant model are described in [14]. A comparison between Saint-Venant and Navier–Stokes solutions is also shown in [15]. This problem is a good example to test the ability of the codes to treat wet–dry interfaces and still water (the sea area before the wave reaches it).

The 2D mesh has 13 541 nodes and 26 000 triangles and the results shown have been obtained with four layers along the vertical direction. The vertical viscosity is $0.1\,\mathrm{m}^2/\mathrm{s}$ and the Strickler coefficient is 30. Figure 10 presents the topography and the initial solution (water level), the maximum initial water depth is approximately 50 m, the initial water level upstream of the dam is 100 m and we assume that the river bed downstream of the dam is dry.

Figures 11 and 12 compare the water depth at $t = 2500$ s obtained by the two models, we can see that the two results are close. We show in Figures 13 and 14 a zoom of the downstream area with the water level and the mean velocity. The results are similar with small discrepancies near the wet–dry interface. The solution obtained with the multilayer is more regular. The CPU times are about 130 min for the multilayer and 400 min for the hydrostatic Navier–Stokes solver.

Finally, we show some details of the solution obtained with the multilayer Saint-Venant model. In Figure 15 a zoom of the upstream area with the water depth and the mean velocity is presented,

DOI: 10.1002/fld

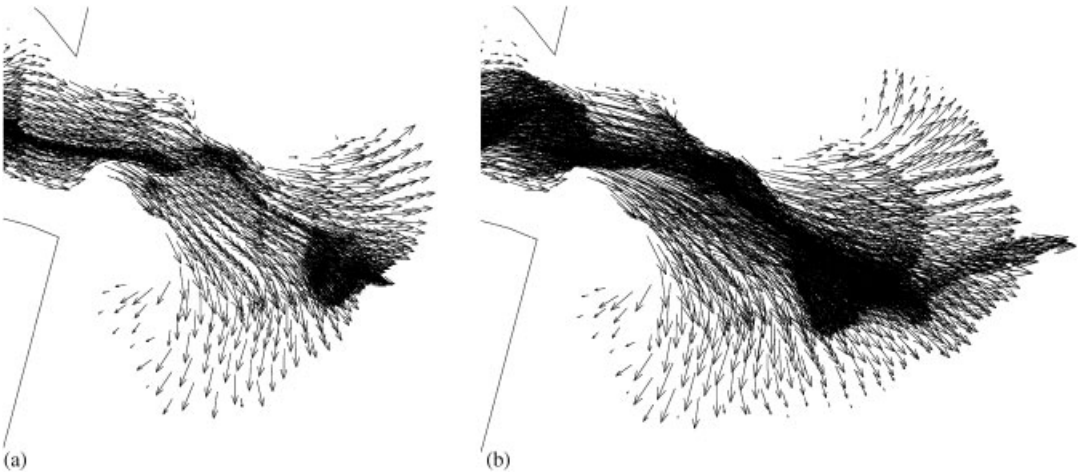

Figure 16. Malpasset, velocity fields: (a) bottom and (b) free surface.

we note that some water is left in the small basins of the topography. For the downstream area, we compare in Figure 16 the velocity field at the bottom and the free surface highlighting the effect of the friction at the bottom.

8. CONCLUSIONS

We have proposed an alternative solution method for the simulation of 3D hydrostatic free surface flows based on Saint-Venant-type systems, which has the main advantage of avoiding to manage a 3D moving mesh. The multilayer model preserves the interesting properties of the kinetic solver applied to the Saint-Venant equations, particularly the water depth positivity and the still water equilibrium. The numerical examples show that we obtain a robust solution method able to deal easily with wet–dry interfaces.

ACKNOWLEDGEMENTS

The authors thank B. Perthame who has been at the origin of this work for helpful discussions. This work was partially supported by EDF/LNHE.

REFERENCES

1. Audusse E. A multilayer Saint-Venant model. *Discrete and Continuous Dynamical Systems*, *Series B* 2005; **5**(2):189–214.
2. Ferrari S, Saleri F. A new two dimensional shallow water model including pressure term and slow varying bottom topography. *M2AN* 2004; **38**(2):211–234.
3. Gerbeau JF, Perthame B. Derivation of viscous Saint-Venant system for laminar shallow water. Numerical validation. *Discrete and Continuous Dynamical Systems*, *Series B* 2001; **1**(1):89–102.
4. Lazzaroni E. Approssimazione numerica di modelli multistrato per fluidi a superficia libera (in Italian). *Tesi di Laurea*, Universita degli studi di Milano, Milan, 2002, http://mox.polimi.it/it/progetti/pubblicazioni

DOI: 10.1002/fld

5. Castro MJ, Garcia-Rodriguez JA, Gonzanlez-Vida JM, Macias J, Pares C, Vazquez-Cendon E. Numerical simulation of two layer shallow water flows through channels with irregular geometry. *Journal of Computational Physics* 2004; **195**:202–235.
6. Hervouet JM. *Hydrodynamique des écoulements à surface libre*; *Modélisation numérique avec la méthode des éléments finis*. Presses des Ponts et Chaussées: Paris, 2003 (in French).
7. Decoene A. Modèle hydrostatique pour les écoulements à surface libre tridimensionnels et schémas numériques. *Thèse*, Université Pierre et Marie Curie, Paris, 2006.
8. Marche F. Theoretical and numerical study of shallow water models. Applications to nearshore hydrodynamics. *Thesis*, Université Bordeaux 1, Bordeaux, 2005.
9. Dal Maso G, LeFloch PG, Murat F. Definition and weak stability of a non conservative product. *Journal de Mathematiques Pures et Appliquees* 1995; **74**:483–548.
10. Audusse E, Bristeau MO. A well-balanced positivity preserving second-order scheme for shallow water flows on unstructured meshes. *Journal of Computational Physics* 2005; **206**:311–333.
11. Audusse E, Bristeau MO. Finite volume solvers for a multilayer Saint-Venant system. *International Journal of Applied Mathematics and Computer Science*, submitted.
12. Audusse E, Bouchut F, Bristeau MO, Klein R, Perthame B. A fast and stable well-balanced scheme with hydrostatic reconstruction for shallow water flows. *SIAM Journal on Scientific Computing* 2004; **25**(6):2050–2065.
13. Bristeau MO, Coussin B. Boundary conditions for the shallow water equations solved by kinetic schemes. *INRIA Report 4282*, 2001, http://www.inria.fr/RRRT/RR-4282.html
14. Hervouet JM. A high resolution 2-D dam-break model using parallelization. *Hydrological Processes* 2000; **14**:2211–2230.
15. Hervouet JM. La résolution des équations de Navier–Stokes non hydrostatiques à surface libre. *Revue Européenne des Éléments Finis* 2003; **12**:143–155.

DOI: 10.1002/fld